Characteristics of acoustic emission signals of Hertzian and unloading cracks in glass

Cite as: Journal of Applied Physics **55**, 2847 (1984); https://doi.org/10.1063/1.333325
Submitted: 23 May 1983 • Accepted: 21 November 1983 • Published Online: 04 June 1998

Kwang Yul Kim and Wolfgang Sachse

Characteristics of acoustic emission signals of Hertzian and unloading cracks in glass

Kwang Yul Kim and Wolfgang Sachse
Department of Theoretical and Applied Mechanics, Cornell University, Ithaca, New York 14853

(Received 23 May 1983; accepted for publication 21 November 1983)

Reproducible acoustic emission (AE) signals can be observed when a spherical diamond indenter is used to generate cone- or ring-shaped Hertzian cracks on the surface of a glass specimen. The signals which are emitted during the loading of the specimen have features virtually indentical to those resulting when a glass capillary is broken on the surface of the specimen. This paper describes the first clear identification of Hertzian cracks which act as point sources of acoustic emission with features corresponding to a vertical force. The temporal characteristics of the force correspond to a Heaviside function with risetime less than 0.1 μs and an amplitude ranging from 1.8×10^{-3} to 4.2×10^{-3} N. The unloading of the diamond indenter from the glass also produces characteristic AE signals. These are distinguishable from the loading signals and they are shown to correspond to the development of unloading cracks on the surface of the specimen. Quantitative information about the unloading cracks is obtained from the AE signals by measuring the amplitude of the first pressure or P wave of the unloading signals. It is shown that this feature is directly related to the maximum applied load attained prior to unloading. A load threshold is found below which no unloading signals are detected.

PACS numbers: 62.20.Mk, 46.30.Nz, 62.65. + k

I. INTRODUCTION

Acoustic emission (AE) techniques appear to be ideal for *in situ* structural integrity monitoring applications. The key to their successful implementation lies in the development of procedures by which the location and characteristics of the emission source can be unambiguously elucidated from the acoustic signals detected by a sensor attached to the surface of a structure. Unfortunately, the characteristics of the source are often obscured by the geometric dispersion effects accompanying the propagating of a broadband transient signal through the structure acting as a waveguide and by the transduction characteristics of the sensor.[1-3]

New approaches for the characterization of the sources of acoustic emission have been vigorously pursued in the recent past. Recognizing that the detected AE signals include the effects of the structure, considerable effort has focused on calculation of the propagation of transient elastic waves in a bounded medium. The case of a point step function of a force applied normal to the surface of a semi-infinite isotropic solid was investigated by Breckenridge *et al.*[4] and compared to the solution of Lamb.[5] The case of a normal force acting on a plate with signals detected at the epicentral position was studied by Hsu *et al.*[6] For this case, the solution obtained by Knopoff[7] can be used. More recently, Pao and co-workers[3,8-10] have provided insight into the AE phenomena by modeling various AE sources in terms of dynamic strain nuclei and by applying generalized ray theory and the method of normal modes to compute, respectively, the signals expected in the near and far fields of a source. A similar approach using a slightly different algorithm was adopted by Simmons and Clough.[11]

Experiments have also been performed with simulated AE sources in a plate structure. Signals from sources such as breaking glass capillaries[4,6] and pencil leads,[2] irradiation by Q-switched laser pulses,[12] chopped electron beams,[13] electrical sparks,[14] and intense beams of x rays[15] have been recorded. It is assumed that each of these simulated sources acts as a point source of specific type. The goal of most of these measurements has been to identify from the detected acoustic signals the nature of the source type and its time function

Reports on the source nature of AE signals emanating from initiating or propagating cracks are fewer. In early work, the recorded signals were used simply to detect the onset of crack formation in a material without regard to the detailed nature of the emitted AE signals associated with it (cf. Ref. 1). Specific AE signal processing procedures such as energy count and amplitude distribution analysis, among others, were developed to detect the formation and growth of cracks in various materials.[16,17] What has been lacking is the fundamental relationship between the characteristics of the AE radiation and features of a forming crack such that its dynamic characteristics could be extracted from the emitted AE signals.

Some attempts to determine this relationship have been reported. In experiments with specimens of austenized mild steel and electrolytic iron in a special "Yobell" geometry designed to act as a half-space, Wadley *et al.*[18] initiated cleavage and intergranular cracks in a localized region of the specimen by deforming it in tension at liquid nitrogen temperature. By assuming the emission source to emit as a dipole, they deconvolved the detected AE signals to obtain source functions of their microcracks. From these source functions they computed a crack opening velocity according to a simple model. Efforts to generate individual crack signals were undertaken by Clough and Simmons[19] who used a Vickers indenter on the surface of a tool steel specimen to produce cracks which were accompanied by reproducable AE signals. It was not clear, however, what type of AE source the generated cracks were. More recently, Wadley and Scruby[20] applied again the dipole force drop model to analyze the AE signals radiated from crack sources in a

 0021-8979/84/082847-10$02.40

wedge opening loading (WOL) specimen subjected to fatigue loading.

In this work we have investigated in detail the acoustic signals emitted when a specific crack type is produced in a brittle material. We have attempted not only to identify the nature of the source of acoustic emission but also to achieve an understanding of the relationship between various parameters of the detected AE signal and the dynamics of the moving crack associated with it.

The experiments to be described were carried out in a brittle, transparent material so that an unambiguous correlation could be made between each crack and its corresponding AE signal. Hertzian cone and other unloading cracks were generated in specimens of soda-lime glass by an indentation technique with a spherical diamond indenter. Acoustic emission signals associated with these cracks were reproducibly detected during the loading and unloading process at one or two receiver locations with a broadband AE system. Special care was taken to achieve reproducibility of the crack generation process as well as of the AE signal detection, recording, and processing.

In the next section of this paper a brief review is given of the characteristics of indentation fracture mechanics and its implications on the generated AE signals. Section III gives a description of the experiments conducted while in Sec. IV are some examples of the results obtained. A discussion of these results is also in this section while some concluding remarks are in Sec. V of this paper.

II. INDENTATION FRACTURE MECHANICS AND AE THEORY

Elastic fields resulting from the elastic contact between two curved bodies can be found described in the works by Hertz.[21] Griffith[22] analyzed the stress concentration around existing microcracks in glass and computed the stress necessary to cause brittle fracture. Roesler[23] extended Griffith's theory of fracture to Hertzian cracks and estimated the specific surface energy of silicate glass. Later, extensions to the theory of Hertzian fracture were developed and tested by Frank and Lawn[24] and Wilshaw.[25] An excellent review on indentation fracture mechanics is in the paper by Lawn and Wilshaw.[26]

In this analysis, an isotropic elastic half-space is subjected to a normal loading force P, applied by a spherical indenter of radius R, as shown in Fig. 1. If the Young's moduli and Poisson's ratios of the specimen and the indenter are, respectively, E, E', and ν, ν', then the radius a of the elastic contact circle is given by[27]

$$a = \left(\frac{4kPR}{3E}\right)^{1/3}, \tag{1}$$

where k is a dimensionless constant given by

$$k = (9/16)[(1-\nu^2) + (1-\nu'^2)E/E']. \tag{2}$$

The maximum tensile stress $\sigma_{rr}^{\max}$ in the specimen occurring at the contact circle is

$$\sigma_{rr}^{\max} = (0.5-\nu)\frac{P}{\pi a^2} = (0.5-\nu)p_0, \tag{3}$$

where $p_0 = P/\pi a^2$ is the mean pressure acting between indenter and specimen. This stress rapidly decreases away from the periphery according to

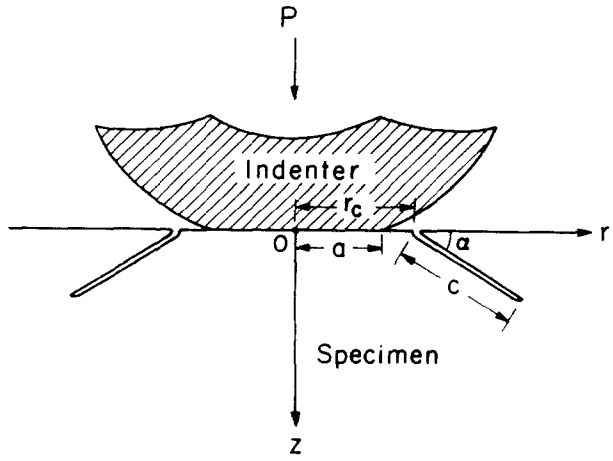

FIG. 1. Sectional view of a Hertzian cone crack formed by a spherical indenter.

$$\sigma_{rr} = (0.5-\nu)p_0(a/r)^2. \tag{4}$$

At some critical load P_c a crack initiates at $r = r_c$ ($r_c \geqslant a$), near the contact circle, probably at the site of an existing microflaw in the specimen. This crack develops in a conical fashion, generally following a trajectory of one of the principal stress directions, to reach a length of c. It can be shown that the formation of such a Hertzian crack, or more generally, any axisymmetric crack, results in a force change in the direction of the applied force. This follows from evaluation of the surface integral, $\int\int \boldsymbol{\sigma}\cdot\mathbf{n}dS$ along the crack path, where $\boldsymbol{\sigma}$ is the stress tensor and $\mathbf{n}$ is an outward normal unit vector of the surface element dS. This integral represents the total tractions acting on the hypothetical crack surface prior to formation of the crack. The surface over which the integration is performed is axisymmetric. For a torsionless axisymmetric case, the stress tensor written in cylindrical coordinates r, θ, and z is given by

$$\boldsymbol{\sigma} = \begin{bmatrix} \sigma_{rr} & 0 & \sigma_{rz} \\ 0 & \sigma_{\theta\theta} & 0 \\ \sigma_{rz} & 0 & \sigma_{zz} \end{bmatrix}, \tag{5}$$

where all the σ_{ij} components are independent of θ.

If a small surface element δ making a slant angle α with the plane normal to z axis is considered, as shown in Fig. 1, then

$$\mathbf{n} = -\sin\alpha\mathbf{r} + \cos\alpha\mathbf{k}, \quad \mathbf{r} = \cos\theta\mathbf{i} + \sin\theta\mathbf{j}, \tag{6}$$

where $\mathbf{r}$, $\mathbf{k}$, $\mathbf{i}$, and $\mathbf{j}$ are unit vectors along the r, z, x, and y directions, respectively. Then

$$\int\int_\delta \boldsymbol{\sigma}\cdot\mathbf{n}dS = \int_0^{2\pi} d\theta \int_\delta \boldsymbol{\sigma}\cdot\mathbf{n}\frac{rdr}{\cos\alpha} \tag{7}$$

$$= \int_0^{2\pi} d\theta \int_\delta [(-\sigma_{rr}\tan\alpha + \sigma_{rz})\mathbf{r} + (\sigma_{zz} - \sigma_{rz}\tan\alpha)\mathbf{k}]rdr. \tag{8}$$

The first and second integrals on the right side of the above equation vanish because of axisymmetry, since all the stresses are independent of θ and $\int_0^{2\pi}\mathbf{r}d\theta = 0$.

If the integration is extended over the entire crack surface Γ then one obtains

$$\int\int_{\Gamma} \boldsymbol{\sigma}\cdot\mathbf{n}dS = 2\pi\mathbf{k}\int(\sigma_{zz} - \sigma_{rz}\tan\alpha)rdr \tag{9}$$

$$= \beta P\mathbf{k}. \tag{10}$$

In the last equation, the magnitude of β is expected to be quite small in comparison with one because of the weak stress field associated with the Eq. (9) outside the contact circle.

In this analysis it can be assumed that the loading system is so soft that the moving crack does not disturb the externally applied force. This is analogous to a constant force loading in fracture dynamics. In other words, the formation of a Hertzian cone crack simply results in a dynamic redistribution of stresses in the specimen without affecting the externally applied force. After formation of a crack, the tractions along the crack surface disappear, and the integrated effect of the disappearance of these tractions over the crack surface results in a change of force in the direction of the externally applied force, according to Eq. (10).

To evaluate the magnitude of this force, Huber's[28] solutions for the stresses σ_{zz} and σ_{rz} appearing in Eq. (9) were used. These are

$$\sigma_{zz} = -1.5\frac{P}{\pi a^2}\left(\frac{z}{\sqrt{u}}\right)^3\frac{a^2u}{u^2+a^2z^2}, \tag{11}$$

$$\sigma_{rz} = -1.5\frac{P}{\pi a^2}\left(\frac{rz^2}{u^2+a^2z^2}\right)\left(\frac{a^2\sqrt{u}}{a^2+u}\right), \tag{12}$$

where

$$u = (1/2)\{(r^2+z^2-a^2) + [(r^2+z^2-a^2)^2 + 4a^2z^2]^{1/2}\}. \tag{13}$$

The surface integral appearing in Eq. (9) was numerically evaluated with the results plotted in Fig. 2 as a function of c/a with r_c/a as a parameter for the angle α of 21°, the value reported in the literature.[26] Since the stress concentration region is localized near the crack tip, this calculation overestimates the magnitude of the force change in the applied loading direction.

The formation of a crack results in an elastic disturbance in the surrounding medium. The domain of the elastic disturbance was initially assumed to be infinite by Mott,[29] but Roberts and Wells[30] later showed that it was bounded. This disturbance is accompanied by elastic wave propagation effects which can be detected as a signal (displacements, velocity, etc.) at the surface of the specimen. For a crack modeled as a jump in displacement, $\|u(\mathbf{x}',t)\|$ at location $\mathbf{x}'$ over a surface S, the waves at the receiver point $\mathbf{x}$ are given by[3,11]

$$u_i(\mathbf{x},t) = \int_{-\infty}^{\infty}dt'\int\int_S \|u_j(\mathbf{x}',t')\|n_k(\mathbf{x}') \times\sum_{jki}(\mathbf{x}-\mathbf{x}',t-t')dS'. \tag{14}$$

Here, $\mathbf{n}'$ is the unit vector normal to the crack surface S. The quantity Σ_{jki} represents Green's stress tensor, which corresponds to the stress tensor at $\mathbf{x}'$ resulting from a concentrated force acting at local $\mathbf{x}$ in the direction x_j. In an equivalent formulation, the integrand of Eq. (14) is expressed as a product of a moment density tensor and the derivative of Green's displacement tensor.[31,32] Furthermore, the surface integral can be converted to a volume integral of the product of an equivalent body force and Green's displacement tensor G_{ij} according to[31]

$$u_i(x,t) = \int_{-\infty}^{\infty}dt'\int\int\int_V f_j(\mathbf{x}',t)G_{ji}(\mathbf{x}|\mathbf{x}',t)dV'. \tag{15}$$

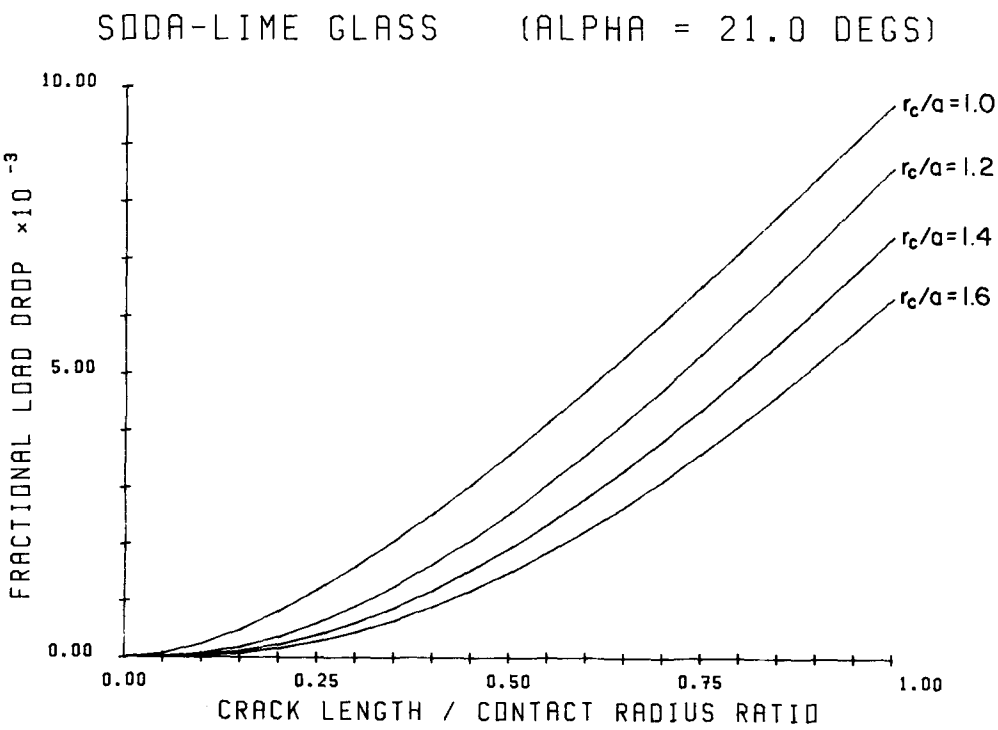

FIG. 2. Calculated fractional load drop as a function of c/a with r_c/a as a parameter for $\alpha = 21°$.

These equivalent body forces f_j are known as nuclei of strains. In this formulation, the various deformation mechanisms are represented either singly or as a combination of strain nuclei. It follows that if the AE source is a point source and the receiver is a point sensor, then all spatial variations at the source and receiver locations can be neglected. In this case, the surface and volume integrals appearing in Eqs. (14) and (15) can be evaluated. The result is of the form

$$u_j(\mathbf{x},t) = \int_0^t f(t')G_j(\mathbf{x},t-t')dt', \quad j = 1,2,3, \tag{16}$$

where G is the appropriate Green's function for the source, structure- and receiver-type, and location. The last equation corresponds to the standard convolution integral of the surface displacement signal given in terms of the source and structure time functions. The evaluation of the Green's function appearing in this analysis has been completed for thick plate structures for various sources in the near-field (up to approximately $6h$, where h is the plate thickness) by the generalized ray theory[3,8,9] and for axisymmetric sources in the far field by the theory of normal modes.[10] The simplest case, corresponding to a vertical step force, with a receiver at the epicentral position on the plate opposite the source was that computed by Knopoff.[7] The expected normal displacement signal, $u_z(t)$ for a step unloading on the surface of a specimen of soda-lime glass is shown in Fig. 3(a). The corresponding normal velocity signals which correspond to the plate impulse response are shown in Fig. 3(b).

The signals detected by a transducer which is not a displacement sensor, but whose transfer characteristics $T(t)$ are used to describe the relationship between signal displacements and output voltage, can be written as a convolution equation in the time domain:

$$V(t) = S(t)*G(t)*T(t), \tag{17}$$

where $V(t)$ is the output signal of the transducer. As shown in our earlier work,[33] it is possible to determine the transfer characteristics of a piezoelectric transducer by carrying out a calibration experiment in which a source of specific type with broadband time characteristics is activated and the output waveform is analyzed.

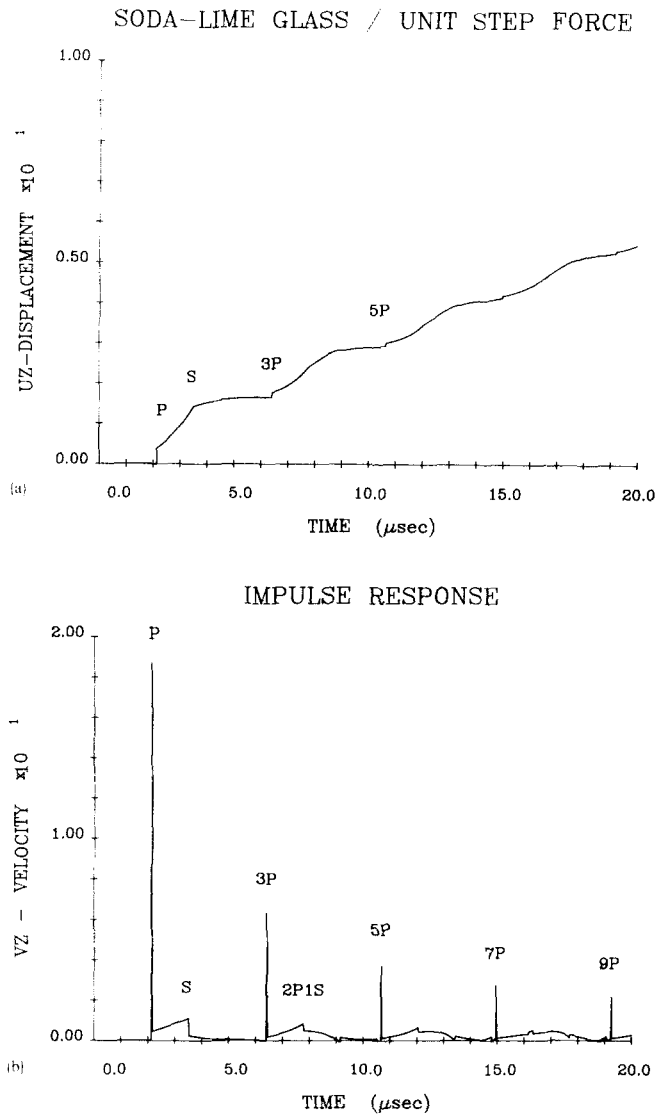

FIG. 3. (a) Theoretical epicentral displacement signal corresponding to a vertical force step source. (b) Calculated epicentral velocity signal corresponding to a vertical force step source.

III. EXPERIMENTS

A. Experimental setup

Hertzian cone and other cracks were reproducibly generated with a spherical diamond indenter of 90-μm radius and a Vickers indenter, which could be attached to a loading frame via a miniature load cell. The loading frame resembled a miniature mechanical testing machine but it was specially constructed to minimize any spurious AE sources. Plastic washers and bushings were inserted at the mechanical joints through which machine noise could be transmitted. To eliminate any frictional noise during the indenter loading and removal, the indenter was moved normal to the specimen with an angular tilt calculated to be less than 10^{-3} deg. The portion of the loading frame where the load cell and indenter are attached is backed by both stiff tensile and compression springs to ensure the stability of the load applied through the indenter. The indenter load cell has a maximum capacity of 225 N with a resolution of 6×10^{-3} N.

Indentation was made onto plate specimens of soda-lime glass with dimensions $10\times10\times1.243$ cm thick. Table I lists the adiabatic Young's modulus and Poisson's ratio of the specimen material which were determined from the measurements of the first P- and S-wave arrivals and the density. Since the calculated difference between the adiabatic and isothermal values for the soda-lime glass is less than 0.1%, it is ignored in the calculation of the fractional force drop β, appearing in Eq. (10). The elastic moduli of the diamond indenter vary with crystallographic direction, but the variation is within 8% from the mean values of Young's modu-

TABLE I. Data for soda-lime glass.

P-wave speed	0.582 cm/μs
S-wave speed	0.355 cm/μs
Density	2.52 g/cm^3
Young's modulus	76.5 GPa
Poisson's ratio	0.20

lus 1.14 TPa and Poisson's ratio 0.07.

The acoustic signals were detected by one or more small broadband point piezoelectric transducers of active area 1.32 mm in diameter. In every case, one such sensor was situated at the epicentral position of the plate, directly beneath the indenter on the opposite side of the plate. In some experiments, a second transducer was located at the distance of $2h$ (h being the thickness of the plate) on the same side as the indenter. System calibration signals were obtained by breaking a glass capillary of inside diameter 0.05 mm and outside diameter 0.08 mm. The glass capillary fracture could be made to occur at the same location as the indentation region by substituting a razor blade in place of the indenter in the loading frame and loading it directly onto the glass capillary.

The transducer output was amplitifed by low-noise preamplifiers which had a frequency response (within 3 dB from 10 kHz to above 2 MHz and a gain of 80 dB. The transducer/amplifier combination had a broadband noise figure of 0.66 μV (rms). The signals were fed into one of two transient recorders of either 8- or 10-bit resolution. These were interfaced to a minicomputer system which permitted interactive processing and storage of the detected AE signals. The electronic block diagram of the system is shown in Fig. 4. There was also provision for digitizing and recording the applied indenter load corresponding to the detected AE signal.

In a complete calibration of an AE system, the exact relationship between specimen surface particle displacements (or velocities) and transducer output signal needs to be established.[34] A more limited calibration of the system is sufficient for the measurements to be described provided that the characteristics of the source are identical in all respects, except in magnitude, to those of the actual source being studied. As will be shown, this is the case here. The relationship between the voltage amplitude of the first P-wave arrival detected by the epicentral transducer and the magnitude of the step unloading force drop obtained by breaking glass capillaries on the surface of the specimen at various load levels was determined. In these experiments, this conversion factor was found to be

$$P\text{-wave amplitude/step force} = 4.61 \times 10^{-3}\ (\text{V/N}). \quad (18)$$

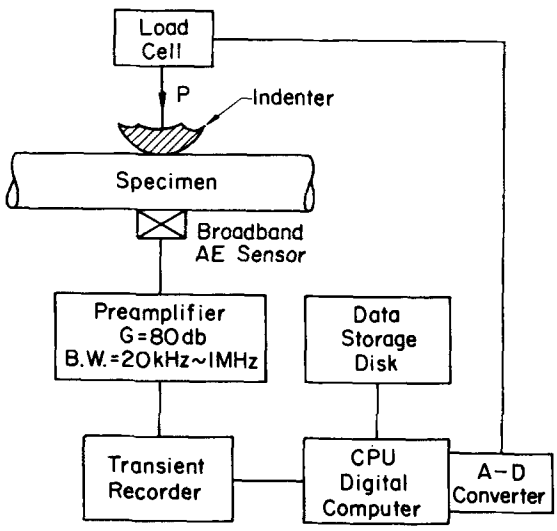

FIG. 4. Electronic block diagram of AE system.

B. Outline of the experiments

In the first set of experiments, the indenter was loaded very slowly up to a level at which the first AE signal associated with Hertzian crack formation was recorded, after which the indenter was gently unloaded. In such loading cycles, no AE signals were observed during the unloading of the indenter. To check the reproducibility, a series of indentations was made in the same way, each time at a new indentation location. The cracks formed on the surface of the glass specimens were examined with an optical microscope after the test to determine the crack size and shape.

In a second set of experiments, progressively higher loads were applied on the indenter above the load at which the first AE signal was detected. The maximum applied load prior to unloading was increased in steps of about 3 N. up to approximately 50 N. During the slow unloading of the indenter, all AE signals emitted were automatically recorded with the data acquisition system together with the corresponding load values.

In a third set of experiments the spherical diamond indenter was replaced by a diamond Vickers indenter which was used to generate loading cracks in the glass plate. Vickers indenter loading signals were recorded for comparison with the loading and unloading AE signals obtained with the sperhical diamond indenter.

IV. RESULTS AND DISCUSSION

Typical waveforms detected by the transducers in the first set of experiments during the loading of the indenter are shown in Figs. 5(a) and 5(b). These figures represent an example of the typical AE signal recorded in the epicentral and $2h$ positions on a soda-lime glass plate during the formation of the first Hertzian cone crack. The signals shown in Figs. 5(a) and 5(b) correspond to a crack formed at load level of 10.33 N. A micrograph of a typical cone crack is shown in Fig. 6. From the digitized waveforms, the crack is estimated to form in less than 0.1 μs which corresponds to ten sample points of the waveform recorder. It also corresponds to the upper frequency limit of the preamplifier used in the measurements.

The signals detected by sensors arranged in a similar configuration as above but with the source a breaking glass capillary, are shown in Figs. 7(a) and 7(b). A comparison of the two corresponding waveforms of crack signals [Fig. 5(a)] and step unloading signals [Fig. 7(a)] shows that they have virtually identical features even in the finest detail up to the arrival of the signals corresponding to the $5P$ wave. This was repeatedly observed. On the basis of this, it is concluded that the formation of an axisymmetric Hertzian cone crack is an AE source of the same type as a breaking glass capillary, that is, an axisymmetric force drop. Small deviations evident after the arrival of the $5P$ wave are likely the result of generating a slightly elliptical cone crack, as can be seen in the

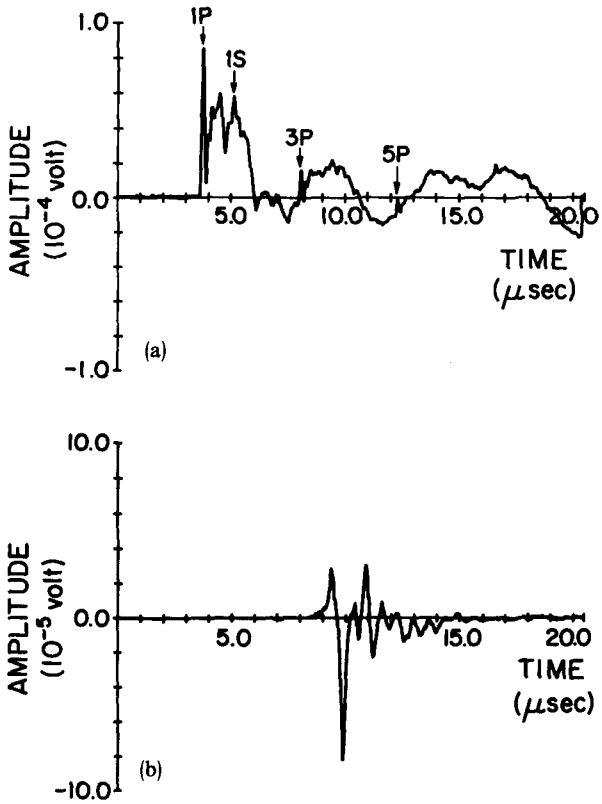

FIG. 5. (a) Epicentral AE signal detected during formation of a Hertzian cone crack. (b) AE signal corresponding to a Hertzian crack detected at the $2h$ position on the source side of the plate.

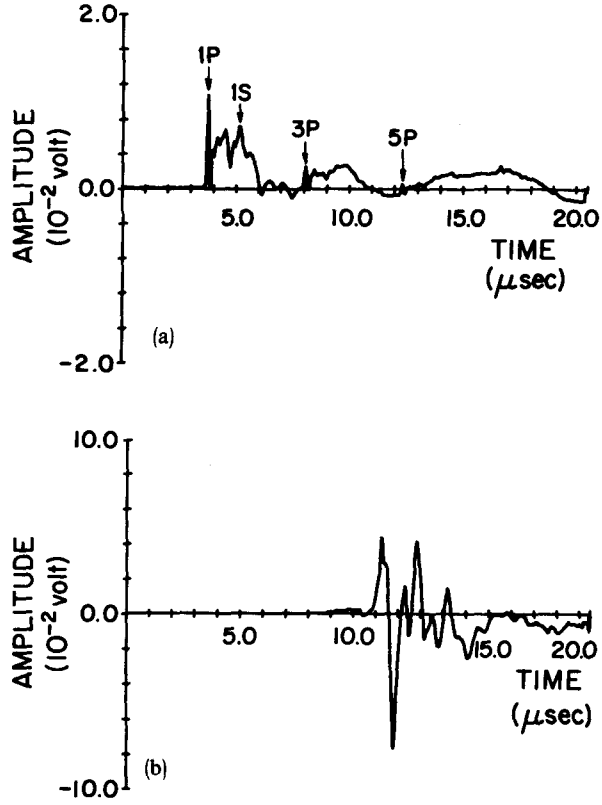

FIG. 7. (a) Epicentral AE signal for a breaking glass capillary. (b) AE signal for a breaking glass capillary detected at the $2h$ position on the source side of the plate.

micrograph shown in Fig. 6. The normal displacement signal $u_z(t)$, detected at the epicenter for the case of a breaking glass capillary source, closely resembles the dynamic Green's function corresponding to a vertical force step source shown in Fig. 3(a), as reported previously.[6,33]

The dimension of the glass capillary used is approximately ten times larger than the length of the crack produced in the indentation. The limiting crack velocity, called the terminal velocity, has been reported to be 0.15 cm/μs in glass.[30] In general, a crack velocity varies along its path. But if an average crack velocity of 0.1 cm/μs is assumed in both specimens, then the rise time of the first P wave of the breaking glass capillary signal should be ten times longer than that of the crack signal. The latter is estimated at 0.1 μs. Since the observed waveforms for both cases exhibit approximately the same rise time, this demonstrates the bandwidth limitations of the amplifiers and waveform recorders comprising the AE system.

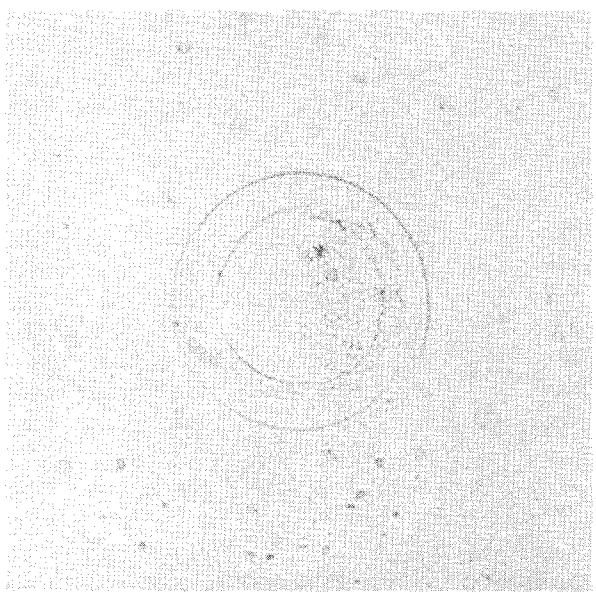

FIG. 6. First formed Hertzian cone crack during loading. Maximum applied load was 8.05 N. Magnification: 665×.

The system calibration factor [Eq. (18)] was used to determine the resultant force change accompanying crack formation from measurement of the first P-wave amplitude. Actually, the use of this calibration factor is not entirely satisfactory, because the transducer used, while appearing to be principally sensitive to the normal component of the surface velocity of the plate, is not a perfect velocity sensor and the rise times of the crack formation and calibration signals are believed to be significantly different. Nevertheless, this scaling can be used to determine the order of magnitude of the force change involved when a Hertzian crack forms and this can be compared to the results obtained from the analytical approach outlined in Sec. II. Table II is a summary of the measurements made of the first observed Hertzian cracks in five tests.

It can be seen from Eqs. (11) and (12), that the Hertzian stress field has the property of geometrical similarity, pro-

TABLE II. Experimental data for Hertzian cracks in soda-lime glass.

Crack number	Applied load P(N)	P-wave amplitude (μV)	Inner cone radius r_c (μm)	Crack length c (μm)	Fractional force drop ($\times 10^4$)
1	9.58	11.4	18.8	8.9	2.58
2	9.11	13.8	19.9	6.0	3.29
3	8.05	8.3	17.7	8.5	2.24
4	9.55	17.4	18.8	8.1	3.96
5	10.34	19.2	17.7	7.7	4.03

vided that all spatial coordinates are normalized to the contact radius a, and all stresses are normalized to the mean contact pressure $p_0 = P/\pi a^2$. Critical to evaluating the indenter-produced stress field in the specimen is the contact radius of the indenter on the surface of the specimen. Since the region under the contact surface is subjected to nearly hydrostatic compression,[27] the increase in elastic moduli of the soda-lime glass is expected to become significant[35,36] around 7.5 GPa, the mean pressure calculated according to Eqs. (1)–(3), which are based on linear elasticity theory at the applied load 9.5 N. This corresponds to a typical load at which first Hertzian crack was observed. The increase in elastic moduli results in a decrease in the contact radius and therefore an increase in the mean pressure. The mean pressure 7.5 GPa corresponding to the applied 9.5 N is thus considered to be a lower limit. The more accurate estimation of contact radius a is quite complicated due to the spatial variation of elastic moduli as a function of pressure under the contact region, while their variation can be safely ignored outside the contact circle, where the stress field is quite weak. Since it was also not possible to measure it directly, it was used as an adjustable parameter in the calculation of the fractional force drop according to Eq. (9).

As can be seen from Table II, a typical fractional force drop, in terms of the applied load, is around 3×10^{-4}. For our test the ratio c/r_c is approximately 0.4. Reported values of r_c/a also scatter around 1.4, ranging from 1.0 to 1.6.[25] With a c/a ratio of 0.4, for instance, Fig. 2 shows that the calculated force drop ranges from 2.5×10^{-3} to 9.0×10^{-4} P as r_c/a varies from 1.0 to 1.6. The experimental data of the measured force drop listed in Table II gives an average value of approximately 3.3×10^{-4} P. As pointed out in Sec. II, the force drop calculation based on Eq. (9) will considerably overestimate the magnitude of force change for cracks of small size, because the region surrounding the crack tip is a region of stress concentration after the crack is arrested.

The duration of the AE source event τ can be computed if it is assumed that the event coincides with the propagating crack and is given by

$$\tau = \int_{r_c}^{r_c + c\cos\alpha} \frac{dr}{v(r)}, \tag{19}$$

where $v(r)$ is the component of the crack velocity along the crack path in the r direction. It is noted that if the receiving transducer were a perfect displacement sensor, then the total rise time of the first P-wave arrival as well as the changing slope of this signal would be closely related to the dynamics of the crack propagation along its path. With the limited bandwidth system used in these experiments, it was impossible to measure the true rate of formation of the Hertzian crack. Clearly, by a judicious combination of a broader bandwidth AE system and an increase in crack size which can be obtained with a larger indenter, this problem would be overcome. The inability to measure a true rise time of the AE events observed was the most unfortunate consequence of using a small indenter in these tests. However, in utilizing a small indenter, a nearly ideal point source of acoustic emission was obtained.

It is noted that in the above description of the crack generation process the overall effect of the cone crack formation results in a vertical force drop even though the instantaneous process of crack initiation and propagation may be modeled as a linear combination of dipole sources with the largest aligned in the direction normal to the crack surface,[32] as has been suggested for the case in Mode I fracture.[20] When a Hertzian cone crack is produced, the cone crack orientation lies close to one of principal stress directions[25] along which the shear stresses vanish; therefore, only the stress normal to the crack surface contributes to the overall dropout of the surface traction as the crack is propagated.

If the load applied through the indenter is gradually increased to levels above which the first Hertzian crack forms, one or more AE signals of the same type but of smaller amplitude as in Fig. 5(a) and 5(b) are observed. This indicates an outward extension of the preexisting cone crack. The same type of signal but of even smaller amplitude is frequently recorded during unloading of the indenter, indicating further growth of the preexisting Hertzian crack or the formation of new, smaller ones. This may be the result of radial tension near the contact region which appears during unloading. The reversal of frictional tractions resulting from the elastic mismatch between the indenter and glass surface at the edge of contact area, enhances radial tension near the contact area. This is consistent with the observations of Johnson *et al.*[37] and Freund.[38]

A second type of a crack was also observed during unloading of the indenter. In the early stages of unloading, sideways extending cracks, termed lateral vents, begin to develop under the influence of the residual stresses around the cone crack beneath the surface. As long as the maximum applied load remains below a certain threshold P_t, these lateral-vent cracks are contained and do not pop out onto the surface of the specimen even after the complete removal of the external load. These lateral-vent cracks could not be detected even with our most sensitive transducers and highest gain amplifiers, possibly because extremely small amplitude AE signals are produced by these cracks and they are buried in the noise of the electronics system (which was less than 1 μV). The transmission micrograph of the crack at this stage is shown in Fig. 8. When the maximum applied load exceeds a load threshold P_t some of these lateral-vent cracks break out to the surface of the specimen during later stages of the unloading process, and they appear to be driven by increased residual stresses. It is often observed that two radially opposite side vents join together, resulting in a crack configuration resembling that of a half-penny crack. Figure 9 shows an example of the transmission micrograph of the crack obtained with maximum applied load of 16.8 N. When the

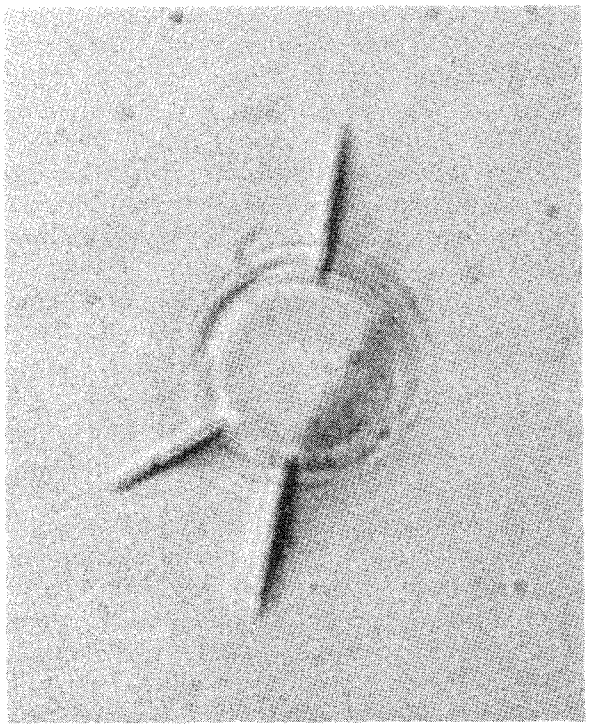

FIG. 8. Lateral vent cracks formed during unloading of the indenter. Maximum applied load was 10.5 N. Magnification: 665×.

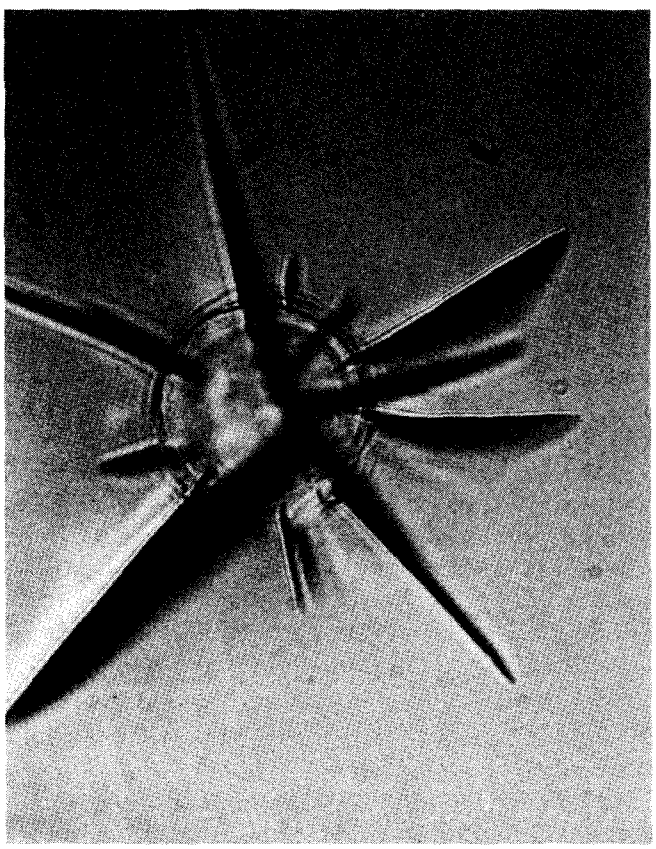

FIG. 9. Many lateral vent cracks including those popped out to the surface of the specimen. Maximum applied load was 16.8 N. Magnification: 665×.

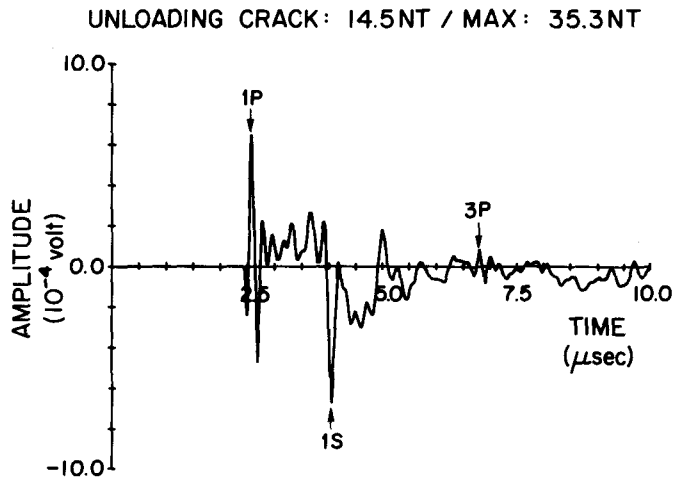

FIG. 10. Epicentral AE signal for the lateral vent crack formed during unloading at 14.5 N. Maximum applied load prior to unloading was 35.3 N.

maximum applied load is much higher than P_t, several mutual intersecting cracks can be observed in the optical microscope.

An example of an epicentral waveform corresponding to this type of an unloading crack is shown in Fig. 10. Inspection of this signal suggests that its source type corresponds to a dipolar force drop caused by the crack opening along the median plane containing the axis with specific θ orientation. During unloading, the residual stresses caused by a mismatch between the elastic and plastic zones give rise to a hoop tension beneath the surface of the specimen which lies outside the contact region.[39,40] This increasing hoop tension is the likely cause of the development of this type of crack. Even if this mechanism is correct, it is not yet possible to compute the expected AE signal since the complex (residual) stress field around the existing cone crack is not yet solved. A detailed analysis of this signal together with acoustic emis-

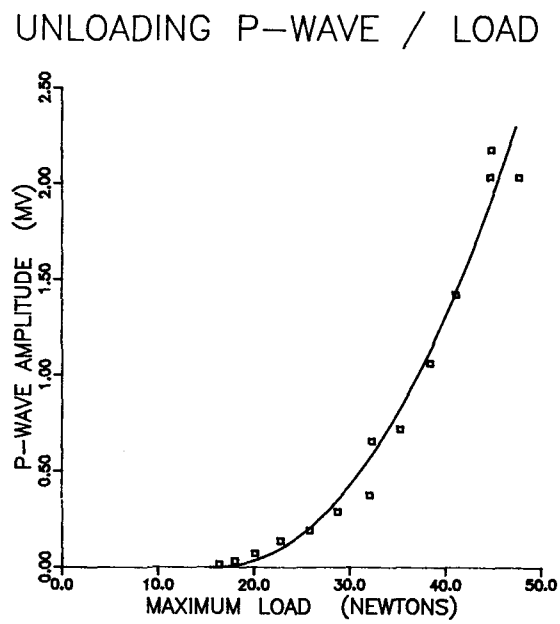

FIG. 11. *P*-wave amplitude of the epicentral AE signal of unloading cracks produced by a spherical indenter vs the maximum applied load during loading.

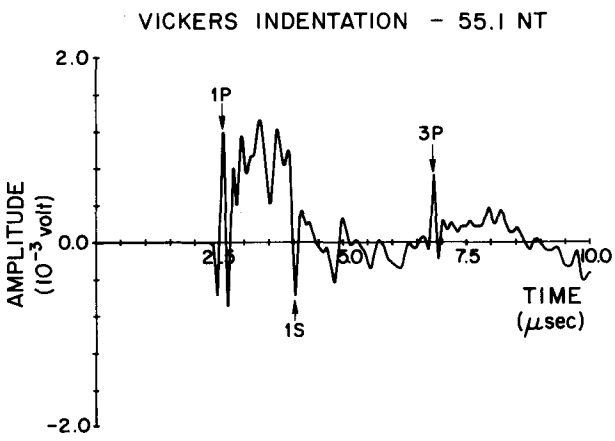

FIG. 12. Epicentral AE signal from a Vickers indenter-generated crack.

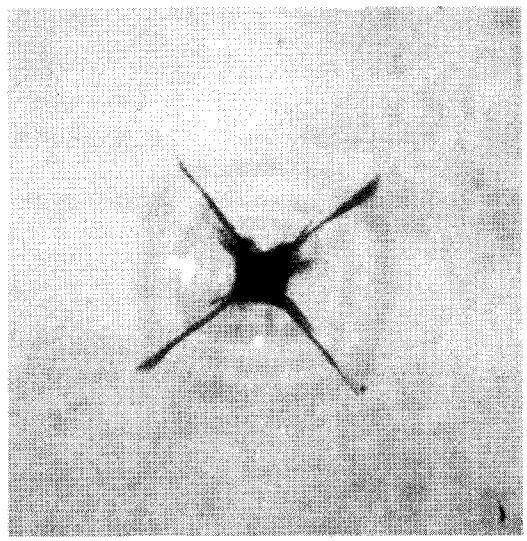

FIG. 13. Cracks produced by a Vickers indenter at 55.1 N load. Magnification: 66.5×.

sions generated during loading using a conical indenter is treated in another paper.[41]

From our experiments, the amplitude A of the first P-wave arrival of the unloading crack signals was measured as a function of maximum applied load prior to unloading P_m with the results plotted in Fig. 11. A nonlinear least squares method was used to fit these data, assuming a power law

$$A = a(P_m - P_t)^n, \tag{20}$$

where the constants a, P_t, and n were determined by the curve fitting. The following values were used to generate the solid line in Fig. 11: $a = 1.37\times10^{-3}$, $n = 2.14$, $P_t = 15.4$ N.

It is noted that the power law is nearly parabolic. The load threshold P_t of about 15 N is the minimum applied load below which fully developed unloading cracks which break through the surface do not form. This was confirmed by visual inspection of the specimen surface.

Finally, for comparison with the previous results, we show in Fig. 12 the typical acoustic signal associated with a crack which has been generated by a Vickers indenter loaded to 55.1 N. The corresponding micrograph is shown in Fig. 13. Two mutually perpendicular median cracks of half-penny configuration can be seen in the micrograph. As described by Lawn and Wilshaw,[26] hoop tension below a Vickers indenter is a major driving force for this crack. The Vickers indenter results in a slightly nonaxisymmetric stress distribution in the specimen. During crack formation, the contribution of the shear stresses $\sigma_{r\theta}$ and $\sigma_{\theta z}$ are expected to significantly affect the fall off of the surface tractions across the crack surface. Thus, the AE source corresponding to this process is expected to be neither of dipolar nor vertical force type, but rather a mixed one. A comparison between the recorded signal shown in Fig. 12 and synthetic AE signals corresponding to the possible source types confirms this.[41]

V. CONCLUSIONS

The following conclusions can be drawn from the work described here.

(1) Reproducible acoustic emission signals can be generated in brittle materials such as soda-lime glass by indentation techniques. During loading, a spherical indenter produces Hertzian cone cracks, and during unloading under certain conditions, lateral vent cracks.

(2) Dynamic processes accompanying the formation of Hertzian or, generally, any axisymmetric crack result in a force change in the direction of the applied load. The time function of this process can be represented by the Heaviside step-force function whose rise time is less than 0.1 μs.

(3) The formation of a Hertzian crack produces acoustic emissions virtually identical to those obtained by breaking a glass capillary on the surface of a specimen. The latter AE source corresponds to a source of normal force type with a Heaviside step time function.

(4) Acoustic emissions accompanying the formation of an unloading crack can be detected when the maximum applied load P_m exceeds a certain threshold value P_t.

(5) The amplitude of the first P-wave arrival in the emitted AE signal associated with the formation of an unloading crack is nearly proportional to $(P_m - P_t)^2$.

(6) The AE signal associated with a loading crack produced by a Vickers indenter on the surface of a glass specimen is very reproducible. The characteristics of this source are neither those of a dipole nor a vertical force drop but rather of a mixed type.

ACKNOWLEDGMENTS

The authors wish to thank Professor Yih-Hsing Pao for his continuing interest in our work. This work was supported by the National Science Foundation through grants to the Materials Science Center and the College of Engineering at Cornell University.

[1] J. Spanner, *Acoustic Emission: Techniques and Applications* (Intex, Evanston, Illinois, 1974), Chap. 3.
[2] N. N. Hsu and S. C. Hardy, in *Elastic Waves and Non-destructive Testing of Materials*, edited by Y. H. Pao (ASME, New York, 1978), AMD-Vol. 29, pp. 85–106.
[3] Y. H. Pao, in *Elastic Waves and Non-destructive Testing of Materials*, edited by Y. H. Pao (ASME, New York, 1978), AMD-Vol. 29 pp. 107–128.
[4] F. R. Breckenridge, C. E. Tschiegg, and M. Greenspan, J. Acoust. Soc. Am. **57**, 626 (1975).

[5]H. Lamb, Philos. Trans. R. Soc. Ser. A **203**, 1 (1904).
[6]N. N. Hsu, J. A. Simmons, and S. C. Hardy, Mater. Eval. **35**, 100 (1977).
[7]L. Knopoff, J. Appl. Phys. **29**, 661 (1958).
[8]Y. H. Pao, R. Gajewski, and A. N. Ceranoglu, J. Acoust. Soc. Am. **65**, 96 (1979).
[9]A. N. Ceranoglu and Y. H. Pao, Trans. ASME **48**, 125 (1981); **48**, 133 (1981).; **48**, 139 (1981).
[10]R. L. Weaver and Y. H. Pao, J. Appl. Mech. **49**, 821 (1982).
[11]J. A. Simmons and R. B. Clough, in *International Conference on Dislocation Modeling of Physical Systems*, edited by J. Hirth and M. Ashby (Pergamon, New York, 1981), pp. 464–467.
[12]C. B. Scruby, R. J. Dewhurst, D. A. Hutchins, and S. B. Palmer, J. Appl. Phys. **51**, 6210 (1980).
[13]G. S. Cargill III, Phys. Today **34**, 27 (1981).
[14]D. Kishoni and W. Sachse, "Spark-Generated Ultrasound," MSC Report No. 4752, Materials Science Center, Cornell University, Ithaca, New York, June 1982.
[15]K. Y. Kim and W. Sachse, Appl. Phys. Letts. **43**, 1099 (1983).
[16]Y. Nakamura, C. L. Veach, and B. O. McCauley, in *Acoustic Emission*, STP 505 (American Society for Testing Materials, Philadelphia, 1972), STP 505, pp. 164–186.
[17]H. Nakasa, in *Advances in Acoustic Emission*, edited by H. L. Dunegan and W. H. Hartman (Dunhart, Knoxville, 1981), pp. 65–86.
[18]H. N. G. Wadley, C. B. Scruby, and G. Shrimpton, Acta. Met. **29**, 399 (1980).
[19]R. B. Clough and J. A. Simmons, Mater. Eval. **39**, 1026 (1981).
[20]H. N. G. Wadley and C. B. Scruby, A.E.R.E. Report R10353, Metallurgy Division, AERE Harwell, December 1981.
[21]H. Hertz, J. Reine Angew. Math. **92**, 156 (1881); Verh. Ver. Befoerderung Gewerbe Fleisses, **61**, 449 (1882), reprinted in English in *Hertz's Miscellaneous Papers* (Macmillan, London, 1896), Chaps. 5 and 6.
[22]A. A. Griffith, Philos. Trans. R. Soc. London Ser. A **221**, 163 (1920).
[23]F. C. Roesler, Proc. Phys. Soc. B **69**, 981 (1956).
[24]F. C. Frank and B. R. Lawn, Proc. R. Soc. Ser. A **229**, 291 (1967).
[25]R. T. Wilshaw, J. Phys. D **4**, 1567 (1971).
[26]B. Lawn and R. Wilshaw, J. Mater. Sci. **10**, 1049 (1975).
[27]S. P. Timoshenko and J. N. Goodier, *Theory of Elasticity*, 3rd ed. (McGraw-Hill, New York, 1970), pp. 409–414.
[28]M. T. Huber, Ann. Phys. **14**, 153 (1904).
[29]N. F. Mott, Engineering **165**, 16 (1948).
[30]D. K. Roberts and A. A. Wells, *Engineering* **24**, 820 (1954).
[31]R. Burridge and L. Knopoff, Bull. Seism. Soc. Am. **34**, 1875 (1964).
[32]K. Aki and P. G. Richards, *Quantitative Seismology: Theory and Methods* (Freeman, San Francisco, 1980) Vol. 1, Chap. 3.
[33]J. Michaels, T. Michaels, and W. Sachse, Mater. Eval. **39**, 1032 (1981).
[34]W. Sachse and N. N. Hsu, in *Physical Acoustics*, edited by W. P. Mason and R. N. Thurston (Academic, New York, 1979), Vol. XIV, pp. 277–406.
[35]J. R. Macdonald, Rev. Mod. Phys. **41**, 316 (1969).
[36]N. Soga, H. Yamanaka, and M. Kunugi, in *High-Pressure Science and Technology: Proceedings of the 6th Airapt Conference*, edited by K. D. Timmerhaus and M. S. Barber (Plenum, New York, 1979), Vol. 2, pp. 200–206.
[37]K. L. Johnson, J. J. O'Connor, and A. C. Woodward, Proc. R. Soc. London Ser. A **334**, 95 (1973).
[38]L. B. Freund, Int. J. Sol. Struct. **14**, 241 (1978).
[39]K. L. Johnson, J. Mech. Phys. Solids **18**, 115 (1970).
[40]C. M. Perrott, Wear **45**, 293 (1977).
[41]K. Y. Kim and W. Sachse, "Characteristic Acoustic Emissions of Penny-shaped Cracks in Glass," MSC Report No. 5136, Materials Science Center, Cornell University, Ithaca, New York, October 1983.